Structure, Vol. 12, 1039–1045, June, 2004, ©2004 Elsevier Ltd. All rights reserved. DOI 10.1016/j.str.2004.04.008

Chromophore Conformation and the Evolution of Tertiary Structural Changes in Photoactive Yellow Protein

Spencer Anderson,[1,3,*] Vukica Srajer,[1,3] Reinhard Pahl,[3] Sudarshan Rajagopal,[1] Friedrich Schotte,[4] Philip Anfinrud,[4] Michael Wulff,[5] and Keith Moffat[1,2,3]

[1]Department of Biochemistry and Molecular Biology
[2]Institute for Biophysical Dynamics
[3]Consortium for Advanced Radiation Sources
University of Chicago
Chicago, Illinois 60637
[4]National Institutes of Health
Bethesda, Maryland 20892
[5]European Synchrotron Radiation Facility
Grenoble Cedex 9
France

Summary

We use time-resolved crystallography to observe the structural progression of a bacterial blue light photoreceptor throughout its photocycle. Data were collected from 10 ns to 100 ms after photoactivation of the E46Q mutant of photoactive yellow protein. Refinement of transient chromophore conformations shows that the spectroscopically distinct intermediates are formed via progressive disruption of the hydrogen bond network to the chromophore. Although structural change occurs within a few nanoseconds on and around the chromophore, it takes milliseconds for a distinct pattern of tertiary structural change to fully progress through the entire molecule, thus generating the putative signaling state. Remarkably, the coupling between the chromophore conformation and the tertiary structure of this small protein is not tight: there are leads and lags between changes in the conformation of the chromophore and the protein tertiary structure.

Introduction

Although the static, ground-state, atomic structures of proteins may be readily characterized both experimentally and computationally, much less is known about the protein dynamics that follow activation of the molecule. Individual static structures designed to mimic each of the dynamic, transient intermediates may be trapped in the crystal, but only time-resolved crystallography allows visualization of the entire structural progression, from the reactant ground state via transient intermediates to a final product state. Chemical or physical events like transient binding of a ligand, absorption of a photon, or covalent phosphorylation initiate such a progression, populate intermediate states, and ultimately modulate the signaling activity of the molecule.

PYP is a very attractive system in which to study the molecular basis of signal transduction since it undergoes a fully reversible, light-induced modification of its chromophore (Cusanovich and Meyer, 2003; Hellingwerf et al., 2003). PYP is a bacterial photoreceptor initially isolated from *Halorhodospira halophila* (Meyer, 1985), which is believed to be involved in a negative phototactic response to blue light (Sprenger et al., 1993). After absorbing a blue light photon, the covalently attached coumaric acid chromophore undergoes *trans* to *cis* isomerization, which initiates a fully reversible photocycle that lasts on the order of 1 s (Figure 1). The photon energy is transduced into a structural signal as the molecule thermally relaxes through a series of spectroscopically distinguishable intermediates, in which the final two intermediates are denoted pR and pB (alternatively, I1 and I2). The lifetimes of successive intermediates progressively increase throughout the photocycle, with that of pR being $\sim$250 μs and of the final intermediate, pB, $\sim$150 ms (Hoff et al., 1994). Although these intermediates are spectroscopically homogeneous, biphasic transition kinetics between them have been observed using both visible and FTIR spectroscopy (Hoff et al., 1994; Xie et al., 2001). Thus, they may not be structurally homogeneous, and the reaction may progress via multiple pathways. Direct interpretation of earlier time-resolved crystallographic data on PYP was hampered by this complex photocycle, in which multiple structural intermediates may overlap in time (Perman et al., 1998; Ren et al., 2001). We focus our study on the E46Q mutant of PYP, an isosteric mutant which exhibits a faster photocycle than wild-type PYP, but one that is simplified in that it apparently follows a single decay pathway (Genick et al., 1997b; Mihara et al., 1997). The mutation replaces a protonated glutamic acid in the chromophore pocket of PYP with glutamine and thereby slightly modifies a key hydrogen bond to the chromophore (Figure 2) (Anderson et al., 2004).

Although the pR intermediate has been extensively studied by multiple techniques, the chromophore conformation of this spectroscopic intermediate has never been accurately refined (Perman et al., 1998; Ren et al., 2001). Time-resolved FTIR data on wild-type PYP predicts the presence of at least two pR chromophore conformations (Brudler et al., 2001), one of which retains the ground-state hydrogen bond network among Tyr42, Glu46, and the chromophore (Borgstahl et al., 1995). The crystal structure of a photostationary state in PYP related to the pB intermediate revealed the chromophore in a *cis* conformation, fully exposed to solvent (Genick et al., 1997a), but did not reveal large changes in tertiary structure distant from the chromophore binding pocket. Subsequent NMR experiments on a related photostationary state in solution, however, revealed significant changes throughout much of the molecule (Rubinstenn et al., 1998, 1999), most notably in the N-terminal cap, helices A, B, and C, the first turn of helix D, parts of β strands I and VI, and the 3_{10} helix to which the chromophore is covalently linked.

We are interested in the high-energy chromophore conformations that harness much of the absorbed pho-

*Correspondence: smander@midway.uchicago.edu

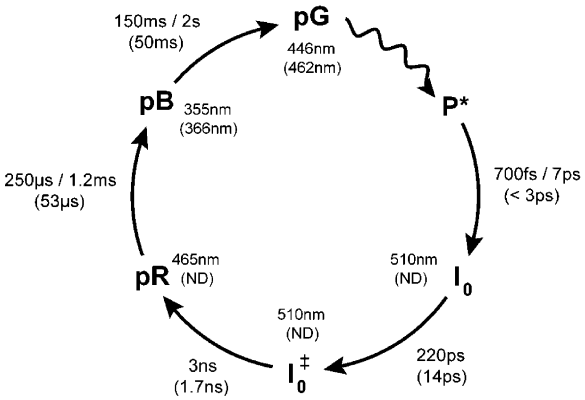

Figure 1. The Room Temperature PYP Photocycle

Absorption maxima and intermediate lifetimes are shown for PYP in solution at neutral pH (Zhou et al., 2001); the values for wild-type (Hoff et al., 1994; Ujj et al., 1998) are listed above those for the E46Q mutant (Genick et al., 1997b; Imamoto et al., 2001b), shown in parentheses. ND, not determined.

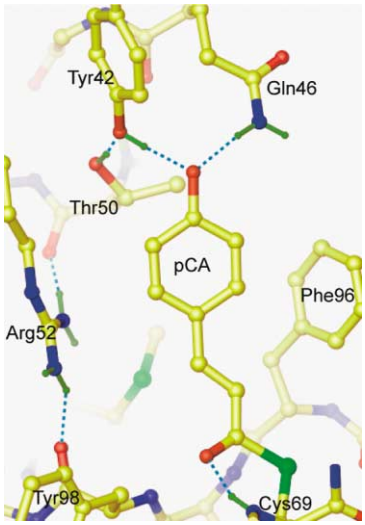

Figure 2. The Ground-State Coumaric Acid Chromophore and Its Binding Pocket in E46Q Mutant PYP

Hydrogen bonds are shown as dashed lines.

ton energy and the global structural changes that occur during the photocycle that might modify interactions of PYP with its putative binding partner(s). In order to develop a comprehensive structural model of the PYP photocycle, significant effort was taken to collect accurate, high-resolution, highly redundant crystallographic data throughout the photocycle that could be used both to clearly visualize very short-lived intermediates and to reveal any small changes in tertiary structure. We report here an extensive time-resolved crystallographic study on the E46Q mutant of PYP as it executes its photocycle, and identify both intermediate chromophore conformations and an unusual pattern of tertiary structural change.

Results and Discussion

Directly Visualizing Structural Change

A total of 54 time-resolved crystallographic Laue data sets (Srajer et al., 1996) were collected at 30 time delays spaced evenly in the logarithm of time from 10 ns to the end of the E46Q mutant photocycle (Table 1). All data were collected on crystals of comparable dimensions and extend to an equivalent resolution, 1.6 Å (see Supplemental Data at http://www.structure.org/cgi/content/full/12/6/1039/DC1). The photocycle was initiated by illumination with a 5–7 ns laser pulse; the laser energy was titrated in order to maximize the number of photons absorbed by the crystal while limiting laser-induced crystal damage. Experiments were performed near room temperature to avoid freezing out the pattern of transient structural change.

The extent of photoactivation in individual datasets varied from ~6% to 34%, which made it difficult to interpret the progression of structural change throughout the data series. We circumvented this problem by averaging datasets in reciprocal space at adjacent time delays to increase the signal-to-noise ratio, effectively increasing data quality at the expense of a reduction in time resolution. This extensive averaging reduced the impact of systematic and random errors, increased overall completeness, and led to difference electron density maps that are clearly more interpretable than any single map (see Supplemental Data). We divided the datasets into eight time regimes (Table 1); the number of time regimes and their temporal extent were chosen to produce a series of maps of comparable quality. Since the data exhibited only a slow evolution of structural change and relatively constant difference electron density, the averaging procedure was particularly advantageous. This data series is also being analyzed by SVD in order to identify intermediate protein structures and their rates of interconversion (S.R. et al., unpublished data). Although SVD has many advantages for interpretation of a time-resolved data series (Schmidt et al.,

Table 1. Crystallographic Data for the Eight Averaged Datasets

Individual Datasets (#)	5	8	10	10	5	5	5	5
Time range	10 ns	100 ns	300 ns	700 ns	10 μs	75 μs	900 μs	7 ms
	40 ns	150 ns	500 ns	5 μs	30 μs	300 μs	3 ms	30 ms
Total observations	456,340	820,816	1,050,181	1,084,273	503,343	470,122	485,793	502,110
Unique observations	13,028	13,628	13,535	13,748	13,107	13,251	13,252	13,225
Redundancy	35	60	78	79	38	35	37	38
Completeness (%)								
100 to 1.60 Å	93.3	97.6	96.9	98.5	93.9	94.9	94.9	94.7
1.67 to 1.60 Å	74.6	89.6	86.2	92.0	74.9	81.3	81.1	79.5

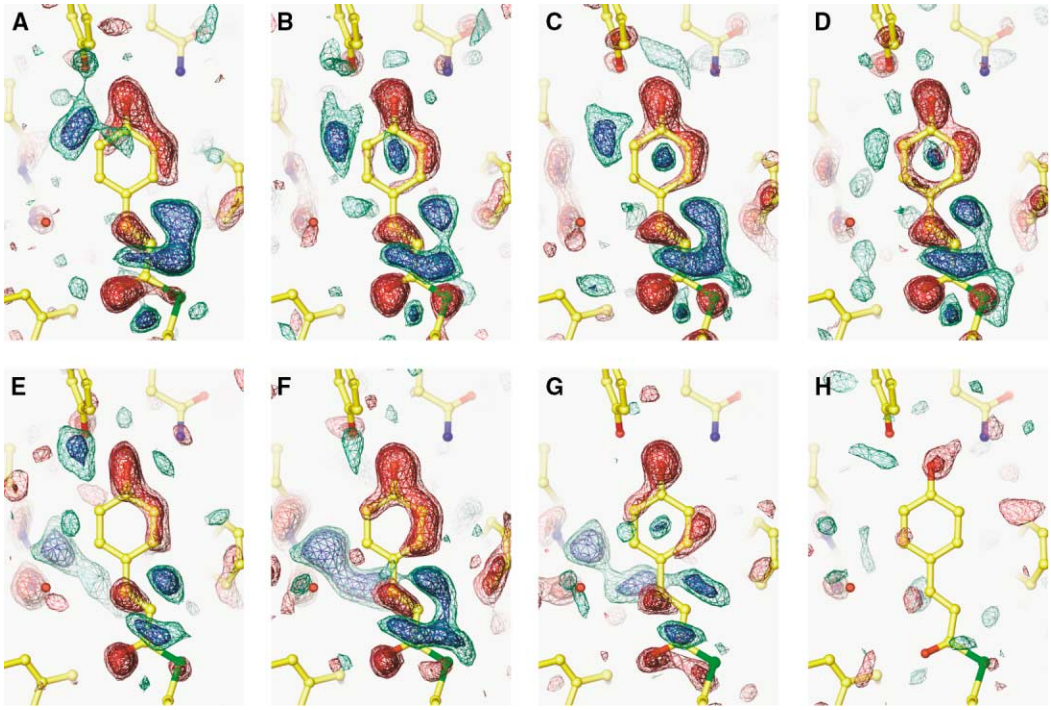

Figure 3. Difference Electron Density Maps of the Chromophore Binding Pocket

Maps show the difference between the illuminated and dark state, superimposed on the ground-state model. Red contours denote negative difference electron density, and blue, positive. The density is contoured at $\pm 2.5\sigma$ and $\pm 3.5\sigma$, where σ is the rms deviation of difference electron density in the asymmetric unit. Averaged time ranges of (A) 10 to 40 ns, (B) 100 to 150 ns, (C) 300 to 500 ns, (D) 700 ns to 5 μs, (E) 10 to 30 μs, (F) 75 to 300 μs, (G) 900 μs to 3 ms, and (H) 7 to 30 ms.

2003, 2004), the weighted averaging in reciprocal space presented here produced maps that were more detailed and easier to interpret.

Intermediate Chromophore Conformations

Only two intermediate chromophore conformations are apparent from 10 ns to the end of the photocycle (Figure 3). We refer to them as the pR and pB chromophore conformations, since they have population dynamics very similar to the corresponding spectroscopic intermediates in solution (Meyer et al., 1987). The pR chromophore conformation is the sole conformation present in the first three averaged maps, from 10 to 500 ns. Although there are slight differences in these maps (compare Figures 3A, 3B, and 3C), the differences are very subtle and cannot be clearly differentiated from noise. This pR conformation coexists with the later pB chromophore conformation in the fourth averaged map, from 700 ns to 5 μs. The pB chromophore conformation is then present in the final four averaged maps, from 10 μs to 30 ms. Nearly all molecules have returned to the ground-state conformation in the final dataset at 100 ms, which was therefore omitted from the averaging.

Since we could not detect any significant evolution of the pR or pB chromophore conformations during the first three (pR) or last four (pB) averaged maps (Figure 3), we further averaged the data in order to generate two extremely high-quality datasets (Table 2) against which the intermediate chromophore conformations could be directly visualized and refined. The fact that this extensive averaging produced chemically plausible chromophore conformations with continuous electron density supports the conclusion that there are only two predominant conformations, one in each of the time domains. Any population with an alternate chromophore conformation would be minor and require data of higher quality to visualize it. The pR intermediate chromophore conformation was refined against a dataset generated by averaging the 23 individual datasets from 10 to 500 ns, and the pB conformation was refined against the average of 15 datasets from 10 μs to 3 ms. Although the

Table 2. Crystallographic Data and Refinement Statistics for Highly Averaged Datasets

Chromophore conformation	pR	pB
Individual datasets (#)	23	15
Time range	10 ns	10 μs
	500 ns	3 ms
Total observations	2,214,726	1,519,242
Unique observations	13,701	13,371
Redundancy	162	114
Completeness (%)		
100 to 1.60 Å	98.1	95.8
1.67 to 1.60 Å	92.4	83.8
Difference R_{cryst}[a] (%)	5.14	6.55
Difference R_{free}[b] (%)	5.96	7.02
PDB accession code	1S1Z	1S1Y

[a] Difference $R_{cryst} = \Sigma_{hkl} ||(F_o^{light} - F_o^{dark}) - (F_c^{light} - F_c^{dark})|| / \Sigma_{hkl} |F_o^{light} - F_o^{dark}|$ includes all data.

[b] Difference R_{free} uses 5% of the data for the test set.

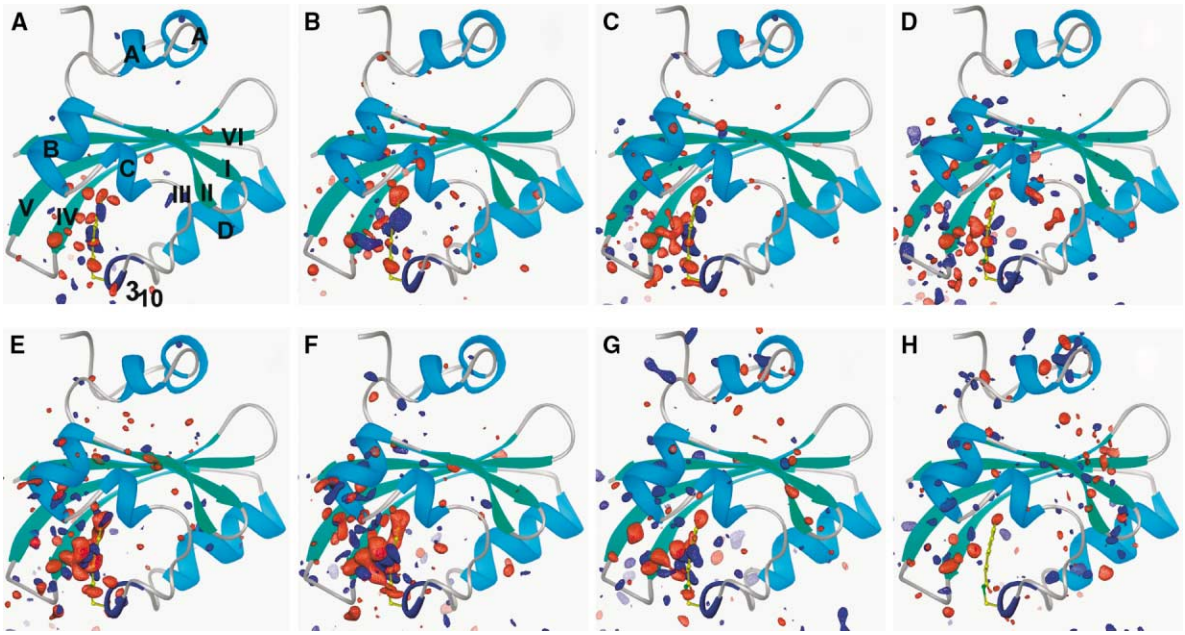

Figure 4. Difference Electron Density Maps of the Entire Molecule
Details as in Figure 2.

chromophore conformations could have been refined against individual, lower quality datasets, the extreme redundancy aided in production of chemically plausible electron density maps of the photoactivated population (see Experimental Procedures and Figure 5). These unbiased electron density maps were critical in accurately refining a transient and potentially strained chromophore conformation for which accurate crystallographic restraints are unknown. We did not refine any residues distant from the chromophore binding pocket, since we detected a range of tertiary conformations associated with each chromophore conformation (Figure 4). Although we concentrate our present refinement on the chromophore and its immediate environment, we are currently characterizing these tertiary conformations by applying singular value decomposition to these data.

The initial stages of the PYP photocycle are dominated by structural rearrangement in direct response to the light-induced *trans* to *cis* isomerization of the chromophore. The ground-state chromophore is in a *trans* conformation in which the position of the chromophore phenolate oxygen is stabilized by two unusually short hydrogen bonds to Glx46 and Tyr42 (Anderson et al., 2004; Borgstahl et al., 1995). This hydrogen bond network becomes strained when the chromophore isomerizes, and its progressive disruption leads to formation of the intermediate chromophore conformations. Although there is evidence of multiple pR conformations in the wild-type PYP photocycle (Brudler et al., 2001; Ren et al., 2001), we visualize only one predominant conformation in the E46Q mutant photocycle. The biphasic relaxation kinetics in the wild-type PYP photocycle may be caused by formation and consequent thermal relaxation of multiple pR chromophore conformations.

In the pR intermediate chromophore conformation, the ground-state hydrogen bond from Gln46 to the chromophore phenolate oxygen is clearly broken (Figure 5C), which allows the phenolate ring to move toward solvent. Despite this significant structural rearrangement, Tyr42 retains its unusually short hydrogen bond to the phenolate oxygen via the displacement of both Tyr42 and Thr50 along with the chromophore. Residues on both sides of the chromophore are displaced to accommodate its *cis* conformation; the Phe96 ring rotates and the Arg52 side chain shifts toward solvent. The position of the Arg52 guanidinium group is stabilized by two hydrogen bonds (both 2.9 Å long) to the backbone carbonyl oxygens of Thr50 and Tyr98 in the ground state (Borgstahl et al., 1995). When the chromophore adopts the pR conformation, these hydrogen bonds are both extended or broken, with new lengths of 3.3 and 3.4 Å, respectively.

The pB intermediate chromophore conformation (Figure 5D) is very similar to that present in a photostationary state of wild-type PYP (PDB entry 2PYP) (Genick et al., 1997a). The remaining hydrogen bond from Tyr42 to the chromophore phenolate oxygen is completely broken. This is the final hydrogen bond to rupture, since it is unusually short in the ground state, ~2.5 Å, which is indicative of a so-called "strong" or "low-barrier" hydrogen bond (Anderson et al., 2004). When this bond breaks, the *cis* chromophore swings into solvent and readily displaces the Arg52 guanidinium group, whose two hydrogen bonds to the adjacent backbone carbonyl groups were already extended in the pR state. The new position of the chromophore phenolic oxygen is too far from the Arg52 guanidinium group to form the hydrogen bond observed in the wild-type photostationary state structure (Genick et al., 1997a), but several new ordered waters are apparent next to the chromophore phenolic oxygen and the Arg52 guanidinium group.

Global Progression of Structural Change

The most striking structural changes evident in the first three maps, from 10 to 500 ns, are restricted to the

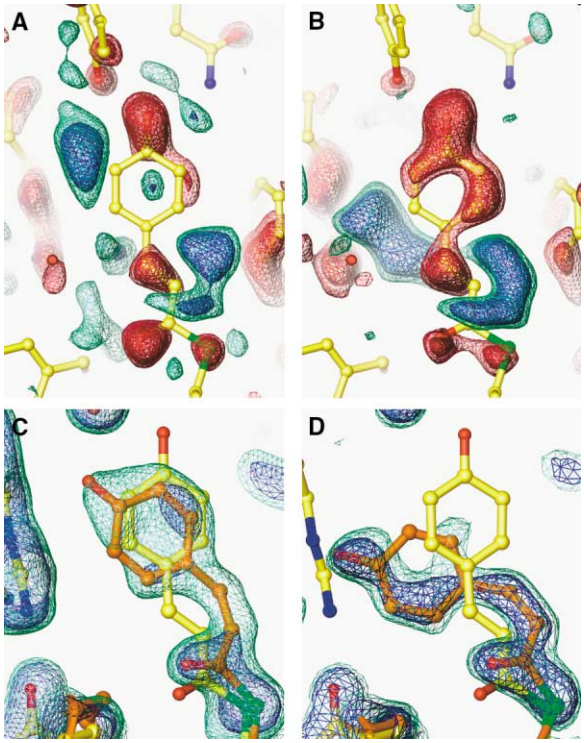

Figure 5. Chromophore Conformations in the pR and pB Intermediates

Difference electron density maps (A and B) and electron density maps (C and D) for the pR and pB chromophore conformations, derived from the two highly averaged data sets (Table 2). Difference electron density contoured at $\pm 2\sigma$ and $\pm 3.5\sigma$, for the (A) pR and (B) pB states. Electron density maps contoured at $\pm 1\sigma$ and $\pm 3\sigma$; yellow atomic model, ground-state conformation; orange models, chromophore conformations for the (C) pR and (D) pB states.

chromophore binding pocket (Figures 4A–4C). There is a slight progression in the extent of structural change throughout this pR time domain, but these changes become more apparent in the fourth map (Figure 4D), when the pB chromophore conformation begins to form. Although the concentration of the pB chromophore conformation first waxes then wanes in the final four maps from 10 μs to 30 ms, the spatial extent of tertiary structural change steadily increases (Figures 4E–4H). Difference electron density features are initially evident in helix B (Figures 4E and 4F), subsequently on the N-terminal helices (Figures 4G and 4H), and finally on the region of the β sheet most distant from the chromophore (Figure 4H). The locations of these features are fully consistent with that visualized in solution using NMR techniques on wild-type PYP (compare Figure 4H in this article with Figure 4 in Rubinstenn et al. [1998]). Although both the E46Q mutation and the protein environment in the crystal reduce the magnitude of tertiary structural changes (Genick et al., 1997a; Xie et al., 2001), our results imply that neither factor qualitatively alters the nature of structural changes occurring within the PYP photocycle.

Although the chromophore has almost completely returned to its *trans* ground-state conformation in the final map from 7 to 30 ms (Figure 4H), this map displays the most prominent difference electron density features distant from the chromophore. Changes in the chromophore conformation thus induce long-range changes in the protein tertiary structure, but our results show that they are not tightly coupled. The *trans* to *cis* isomerization of the PYP chromophore upon photon absorption occurs in much less than one nanosecond, a rapid motion that forces neighboring residues like Tyr42, Glu46, Thr50, Arg52, and Phe96 to move on a similar time scale. In contrast, we see that the indirect rearrangements initiated by rupture of the hydrogen bond network are much slower and follow a microsecond to millisecond time scale (akin to rates observed in protein folding [Englander, 2000]). PYP therefore uses a rapid, light-driven motion of a cofactor to introduce strain and thereby initiate much slower, but spatially more extensive, rearrangement of the surrounding protein.

Surprisingly, we observe the greatest spatial extent of tertiary structural change after the chromophore has reisomerized to *trans* and moved to its ground-state location. A few small difference electron density features remain in the chromophore binding pocket in the final map (Figure 4H). Since these features overlay the strongest difference electron density peaks created by the pB conformation (Figure 4G), they are likely to arise from a small, residual population of molecules whose chromophore remains in the pB conformation. The fact that tertiary structural changes significantly lag behind those at the chromophore implies it takes some time for the protein to fully sense the pB chromophore conformation and shift accordingly. This same quality is observed in wild-type PYP in solution: the chromophore first assumes its protonated pB conformation before subsequent global structural changes expose a region that is capable of binding a hydrophobic dye (Hendriks et al., 2002). This loose coupling between the chromophore conformation and tertiary structure is especially apparent in the E46Q mutant because of its faster photocycle compared to wild-type. The lifetime of the pB chromophore conformation is much shorter in the mutant (Figure 1), perhaps because the mutant does not have to reprotonate residue 46 in order to regain the ground state. Thus, the tertiary structural changes are still developing in the mutant when the chromophore reisomerizes to the *trans* ground state. This accounts for the observation that the E46Q mutant has a reduced extent of tertiary structural change in solution (Xie et al., 2001): the chromophore does not remain in its pB conformation long enough for the tertiary structural changes to fully develop.

The pB conformation is the putative signaling state of PYP, in which the most prominent structural changes include exposure of hydrophobic regions and tertiary structural changes that have been described as partial unfolding (Lee et al., 2001; Rubinstenn et al., 1998; Xie et al., 2001). As observed in solution on both wild-type PYP and the E46Q mutant (Brudler et al., 2001; Xie et al., 2001), only very limited tertiary structural changes occur prior to formation of the pB intermediate (Figures 4A–4C). The chromophore conformation regulates acquisition of this protein conformation by stabilizing the protein in its ground state; the protein can only develop into the biological signaling state upon photon absorption. The *trans* to *cis* isomerization of the chromophore provides a means to transiently rupture these stabilizing

elements, of which the most notable is the hydrogen bond network to the chromophore phenolate oxygen. Indeed, structural instability similar to that found in the tertiary pB conformation can be created artificially in the ground state by significantly weakening the links between the chromophore and rest of the protein. For example, the PYP apoprotein lacks a chromophore and is substantially unstable and prone to denaturation, while removing the unusually short hydrogen bond to the chromophore, as in the Y42F and Y42A mutants, greatly destabilizes the ground state (Brudler et al., 2000; Imamoto et al., 2001a).

The initial stages of light-driven signal transduction observed in PYP may be analogous to that in another PAS domain protein, the FMN-containing LOV2 domain from the plant blue light photoreceptor, phototropin (Crosson et al., 2003). Despite very different chromophores, photoactivation of both PYP and LOV2 leads to a similar tertiary structural change in which one or more α helices flanking the central β sheet are destabilized (Harper et al., 2003; Rubinstenn et al., 1998). The structural changes in PYP are initiated by chromophore isomerization, while those in phototropin LOV2 by formation of a transiently stable covalent bond between the FMN chromophore and a nearby cysteine side chain (Crosson and Moffat, 2002). Photoactivation has opposite effects in the chromophore binding pocket of the two proteins. Chromophore isomerization in PYP ruptures the hydrogen bond network, a critical, preexisting structural linkage, but a completely new structural linkage is formed in LOV2 via the covalent bond between FMN and the protein. Despite this large difference in the underlying chemistry, both initiate a pattern of structural change in the protein that ultimately propagates to the surface of the molecule (Crosson et al., 2003), where it can be sensed by a downstream partner.

Conclusion

Our time-resolved structural study on the PYP photoreceptor has detailed a specific mode of signal transduction. The high resolution and quality of the extensively averaged, time-resolved crystallographic data allow us to unambiguously assign the structure of the chromophore conformation in the two principal spectroscopic intermediates in the PYP photocycle. We directly observe the progression of global structural changes as the protein evolves from its ground to signaling state and demonstrate that the nature of these changes in the crystal are consistent with those in solution. Although previous studies in both solution and crystal (Brudler et al., 2001; Perman et al., 1998; Ren et al., 2001) endeavored to identify the conformation of the chromophore in the pR intermediate, this is the first time such a novel species with a submicrosecond lifetime has been clearly visualized and accurately refined at room temperature. The ability to visualize detailed structural changes as a protein progresses from its ground to signaling state and back again broadens our understanding of how proteins are able to transmit environmental stimuli into a biological response.

Experimental Procedures

Laue Data Collection

All crystals were prepared as described (Anderson et al., 2004). The crystals chosen for data collection were $\sim$180 $\times$ 180 $\times$ 500 μm. Diffraction data were collected either at the BioCARS beamline 14ID-B, the Advanced Photon Source, or the European Synchrotron Radiation Facility beamline ID09. Crystal temperature was kept at 297 K for all experiments. The exact data collection protocol depended on the time delay and the synchrotron bunch mode (see Supplemental Data).

Photoactivation

Crystals were photoactivated using an Nd:YAG laser to pump either a dye laser with Coumarin 500 dye or an optical parametric oscillator, producing a 7 or 5 ns FWHM pulse, respectively (see Supplemental Data). The laser spot profile was approximately 1 mm in diameter at the crystal for all data sets. Laser pulse energy was varied between datasets to ensure maximum photoactivation. The pulse energy was titrated upwards to the maximum value at which the images could be processed. Above this value, crystal twitching between exposures caused elongated diffraction spots that could not be accurately quantitated.

Data Averaging

Redundant datasets were merged in reciprocal space using weighted averaging of ΔF values. The weight was related to the standard error, σ, of ΔF: weight $= 1/(1 + \sigma^2/<\sigma^2>)$ (Ursby and Bourgeois, 1997). The unique reflections present only in a single dataset were retained in order to increase completeness. The influence of poorly measured ΔF values on the Fourier series can be minimized by weighting (Ren et al., 2001), but after sufficient averaging, the weighting of ΔF values was no longer necessary or helpful in visualizing the difference electron density signal.

Generating Maps of the Photoactivated Population

Electron density maps of the photoactivated population were generated to assist in model building and assessment of refinement. These maps were generated by multiplying ΔF by a factor related to occupancy of the photoactivated state before adding to F_c^{dark}: (2/photoactive occupancy) $\times$ ($F_o^{light} - F_o^{dark}$) + F_c^{dark}. The difference between F_o^{dark} and F_c^{dark} is the residual of the ground-state refinement; the final map thus represents the electron density of the photoactivated population minus the ground-state residual. The phases were taken from the simulated annealing, 1.10 Å room temperature E46Q structure with the chromophore omitted (Anderson et al., 2004).

Data Processing and Refinement

All indexing, integration, scaling, and merging was performed using LaueView (Ren and Moffat, 1995). Model building was performed using XtalView (McRee, 1999), and refinement with SHELX97 (Sheldrick, 1997). All refinement was performed as difference refinement in reciprocal space (Terwilliger and Berendzen, 1995). The intermediate chromophore coordinates were initially refined with occupancy and B values fixed. After convergence of the intermediate structure, the occupancy was refined along with the intermediate atomic positions. Distance, angle, and planarity restraints in the chromophore tail were gradually relaxed, and finally the isotropic B value was refined.

The value of R free was monitored to assess the progress of refinement, but the absolute value of this parameter was of limited usefulness in difference refinement. The same set of reflections was used for all intermediate refinements. Progress was also critically assessed using residual electron density maps; we aimed to account for all significant electron density features.

Acknowledgments

We thank Hyotcherl Ihee, Jason Key, and Marius Schmidt for their support during data collection and technical advice. This work was supported by National Institutes of Health Grant GM36452 (K.M.); the BioCARS facility at the Advanced Photon Source is supported by National Institutes of Health Grant RR07707 (K.M.).

Received: February 26, 2004
Revised: April 1, 2004
Accepted: April 5, 2004
Published: June: 8, 2004

References

Anderson, S., Crosson, S., and Moffat, K. (2004). Short hydrogen bonds in photoactive yellow protein. Acta Crystallogr. D Biol. Crystallogr., *60*, 1008–1016.

Borgstahl, G.E., Williams, D.R., and Getzoff, E.D. (1995). 1.4 A structure of photoactive yellow protein, a cytosolic photoreceptor: unusual fold, active site, and chromophore. Biochemistry *34*, 6278–6287.

Brudler, R., Meyer, T.E., Genick, U.K., Devanathan, S., Woo, T.T., Millar, D.P., Gerwert, K., Cusanovich, M.A., Tollin, G., and Getzoff, E.D. (2000). Coupling of hydrogen bonding to chromophore conformation and function in photoactive yellow protein. Biochemistry *39*, 13478–13486.

Brudler, R., Rammelsberg, R., Woo, T.T., Getzoff, E.D., and Gerwert, K. (2001). Structure of the I1 early intermediate of photoactive yellow protein by FTIR spectroscopy. Nat. Struct. Biol. *8*, 265–270.

Crosson, S., and Moffat, K. (2002). Photoexcited structure of a plant photoreceptor domain reveals a light-driven molecular switch. Plant Cell *14*, 1067–1075.

Crosson, S., Rajagopal, S., and Moffat, K. (2003). The LOV domain family: photoresponsive signaling modules coupled to diverse output domains. Biochemistry *42*, 2–10.

Cusanovich, M.A., and Meyer, T.E. (2003). Photoactive Yellow protein: a prototypic PAS domain sensory protein and development of a common signaling mechanism. Biochemistry *42*, 965–970.

Englander, S. (2000). Protein folding intermediates and pathways studied by hydrogen exchange. Annu. Rev. Biophys. Biomol. Struct. *29*, 213–238.

Genick, U.K., Borgstahl, G.E., Ng, K., Ren, Z., Pradervand, C., Burke, P.M., Srajer, V., Teng, T.Y., Schildkamp, W., McRee, D.E., et al. (1997a). Structure of a protein photocycle intermediate by millisecond time-resolved crystallography. Science *275*, 1471–1475.

Genick, U.K., Devanathan, S., Meyer, T.E., Canestrelli, I.L., Williams, E., Cusanovich, M.A., Tollin, G., and Getzoff, E.D. (1997b). Active site mutants implicate key residues for control of color and light cycle kinetics of photoactive yellow protein. Biochemistry *36*, 8–14.

Harper, S., Neil, L., and Gardner, K. (2003). Structural basis of a phototropin light switch. Science *301*, 1541–1544.

Hellingwerf, K.J., Hendriks, J., and Gensch, T. (2003). Photoactive yellow protein, a new type of photoreceptor protein: will this "yellow lab" bring us where we want to go? J. Phys. Chem. A *107*, 1082–1094.

Hendriks, J., Gensch, T., Hviid, L., van der Horst, M.A., Hellingwerf, K.J., and van Thor, J.J. (2002). Transient exposure of hydrophobic surface in the photoactive yellow protein monitored with Nile red. Biophys. J. *82*, 1632–1643.

Hoff, W.D., van Stokkum, I.H., van Ramesdonk, H.J., van Brederode, M.E., Brouwer, A.M., Fitch, J.C., Meyer, T.E., van Grondelle, R., and Hellingwerf, K.J. (1994). Measurement and global analysis of the absorbance changes in the photocycle of the photoactive yellow protein from *Ectothiorhodospira halophila*. Biophys. J. *67*, 1691–1705.

Imamoto, Y., Koshimizu, H., Mihara, K., Hisatomi, O., Mizukami, T., Tsujimoto, K., Kataoka, M., and Tokunaga, F. (2001a). Roles of amino acid residues near the chromophore of photoactive yellow protein. Biochemistry *40*, 4679–4685.

Imamoto, Y., Mihara, K., Tokunaga, F., and Kataoka, M. (2001b). Spectroscopic characterization of the photocycle intermediates of photoactive yellow protein. Biochemistry *40*, 14336–14343.

Lee, B.C., Croonquist, P.A., Sosnick, T.R., and Hoff, W.D. (2001). PAS domain receptor photoactive yellow protein is converted to a molten globule state upon activation. J. Biol. Chem. *276*, 20821–20823.

McRee, D.E. (1999). XtalView Xfit: a versatile program for manipulating atomic coordinates and electron density. J. Struct. Biol. *125*, 156–165.

Meyer, T.E. (1985). Isolation and characterization of soluble cytochromes, ferredoxins and other chromophoric proteins from the halophilic phototrophic bacterium *Ectothiorhodospira-Halophila*. Biochim. Biophys. Acta *806*, 175–183.

Meyer, T.E., Yakali, E., Cusanovich, M.A., and Tollin, G. (1987). Properties of a water-soluble, yellow protein isolated from a halophilic phototrophic bacterium that has photochemical activity analogous to sensory rhodopsin. Biochemistry *26*, 418–423.

Mihara, K., Hisatomi, O., Imamoto, Y., Kataoka, M., and Tokunaga, F. (1997). Functional expression and site-directed mutagenesis of photoactive yellow protein. J. Biochem. (Tokyo) *121*, 876–880.

Perman, B., Srajer, V., Ren, Z., Teng, T., Pradervand, C., Ursby, T., Bourgeois, D., Schotte, F., Wulff, M., Kort, R., et al. (1998). Energy transduction on the nanosecond time scale: early structural events in a xanthopsin photocycle. Science *279*, 1946–1950.

Ren, Z., and Moffat, K. (1995). Quantitative-analysis of synchrotron Laue diffraction patterns in macromolecular crystallography. J. Appl. Crystallogr. *28*, 461–481.

Ren, Z., Perman, B., Srajer, V., Teng, T.Y., Pradervand, C., Bourgeois, D., Schotte, F., Ursby, T., Kort, R., Wulff, M., and Moffat, K. (2001). A molecular movie at 1.8 A resolution displays the photocycle of photoactive yellow protein, a eubacterial blue-light receptor, from nanoseconds to seconds. Biochemistry *40*, 13788–13801.

Rubinstenn, G., Vuister, G.W., Mulder, F.A.A., Dux, P.E., Boelens, R., Hellingwerf, K.J., and Kaptein, R. (1998). Structural and dynamic changes of photoactive yellow protein during its photocycle in solution. Nat. Struct. Biol. *5*, 568–570.

Rubinstenn, G., Vuister, G.W., Zwanenburg, N., Hellingwerf, K.J., Boelens, R., and Kaptein, R. (1999). NMR experiments for the study of photointermediates: application to the photoactive yellow protein. J. Magn. Reson. *137*, 443–447.

Schmidt, M., Rajagopal, S., Ren, Z., and Moffat, K. (2003). Application of singular value decomposition to the analysis of time-resolved macromolecular X-ray data. Biophys. J. *84*, 2112–2129.

Schmidt, M., Pahl, R., Srajer, V., Anderson, S., Ren, Z., Ihee, H., Rajagopal, S., and Moffat, K. (2004). Protein kinetics: structure of intermediates and reaction mechanism from time-resolved X-ray data. Proc. Natl. Acad. Sci. USA, in press.

Sheldrick, G. (1997). SHELXL97 (Göttingen, Germany: University of Göttingen).

Sprenger, W.W., Hoff, W.D., Armitage, J.P., and Hellingwerf, K.J. (1993). The eubacterium *Ectothiorhodospira halophila* is negatively phototactic, with a wavelength dependence that fits the absorption spectrum of the photoactive yellow protein. J. Bacteriol. *175*, 3096–3104.

Srajer, V., Teng, T.Y., Ursby, T., Pradervand, C., Ren, Z., Adachi, S., Schildkamp, W., Bourgeois, D., Wulff, M., and Moffat, K. (1996). Photolysis of the carbon monoxide complex of myoglobin: nanosecond time-resolved crystallography. Science *274*, 1726–1729.

Terwilliger, T.C., and Berendzen, J. (1995). Difference refinement: obtaining differences between 2 related structures. Acta Crystallogr D Biol. Crystallogr. *51*, 609–618.

Ujj, L., Devanathan, S., Meyer, T.E., Cusanovich, M.A., Tollin, G., and Atkinson, G.H. (1998). New photocycle intermediates in the photoactive yellow protein from *Ectothiorhodospira halophila*: picosecond transient absorption spectroscopy. Biophys. J. *75*, 406–412.

Ursby, T., and Bourgeois, D. (1997). Improved estimation of structure-factor difference amplitudes from poorly accurate data. Acta Crystallogr. A *53*, 564–575.

Xie, A., Kelemen, L., Hendriks, J., White, B.J., Hellingwerf, K.J., and Hoff, W.D. (2001). Formation of a new buried charge drives a large-amplitude protein quake in photoreceptor activation. Biochemistry *40*, 1510–1517.

Zhou, Y., Ujj, L., Meyer, T.E., Cusanovich, M.A., and Atkinson, G.H. (2001). Photocycle dynamics and vibrational spectroscopy of the E46Q mutant of photoactive yellow protein. J. Phys. Chem. A *105*, 5719–5726.

Accession Numbers

Coordinates for both structures have been deposited in the Protein Data Bank under accession codes 1S1Z and 1S1Y.